Semiflexible polymer solutions. I. Phase behavior and single-chain statistics

Andrew J. Spakowitz and Zhen-Gang Wang
Division of Chemistry and Chemical Engineering, California Institute of Technology, Pasadena, California 91125

(Received 1 August 2003; accepted 30 September 2003)

We study the thermodynamics and single-chain statistics of wormlike polymer solutions with Maier–Saupe-type interactions using self-consistent-field (SCF) theory. The SCF equations are derived using a systematic field-theoretical approach which yields the SCF equations as the lowest order approximation, but permits fluctuation corrections to be incorporated. We solve the SCF equations using the spheroidal functions, which provides a nonperturbative description of the thermodynamics and single-chain statistics in the nematic state for arbitrary degrees of nematic order. Several types of phase diagrams are predicted, with an emphasis on the limit of metastability (spinodal) associated with each phase. The shape and location of these spinodals suggest interesting scenarios for the phase transition kinetics. A large but finite persistence length is shown to significantly decrease the isotropic–nematic transition temperature relative to that for rigid rods. In the nematic state, the mean-square end-to-end distance in the parallel and perpendicular directions are governed by two separate correlation lengths. An exact relationship between these correlation lengths and the eigenvalues of the spheroidal functions is provided, which reproduces the analytical expressions predicted from earlier studies in the limit of large nematic strength. The dominant contribution to the single-chain thermodynamics is shown to arise from small amplitude undulations in the directions perpendicular to the nematic direction; the presence of hairpins, though crucial for determining the dimensions of the polymer, has insignificant consequences on the single-chain thermodynamics. © *2003 American Institute of Physics.* [DOI: 10.1063/1.1628669]

I. INTRODUCTION

Polymers with sufficient backbone bending rigidity can form nematic liquid crystalline phases at low temperatures and/or high concentrations. The enhanced alignment of the polymer chains in the nematic state is the basis for several material properties and processes such as high strength fibers[1] and flow induced crystallization.[2–6] Solutions of DNA form lyotropic liquid crystalline phases under several biologically relevant conditions including molecular crowding,[7] large molecular weight,[8] polycationic agents (synthetic[9] and natural[10]), and supercoiling in plasmid DNA.[11] Thus the nematic state of main-chain liquid crystalline polymers is a subject of importance in both materials science and biology.

In this paper, we study the nematic phase of solutions of semiflexible polymers: polymers with a backbone of uniform, finite stiffness. In contrast to the simpler case of rigid rods where nematic ordering is associated with only a loss of the rotational degrees of freedom, the nematic state of semiflexible polymers is accompanied by a loss of both the overall rotational entropy of the chain and the conformation entropy of the chain segments. The conformation degrees of freedom lead to two important effects. At length scales less than the natural persistence length, the undulation of the chain backbone acts to weaken the aligning interactions between neighboring molecules and is thus expected to affect the nematic ordering of the chains. At larger length scales, for sufficiently long chains, the polymer can undergo sharp reversals in direction to form hairpin defects.[12] The presence of hairpins in liquid-crystalline polymers has profound effects on the chain dimensions[13,14] and the elastic behavior[15] of the nematic state. The finite bending rigidity of the chains has also been suggested as being responsible for the unusual rheological behavior of nematic liquid-crystalline polymers, such as shear-induced banding.[16]

We examine the phase behavior and conformation properties of lyotropic polymer liquid crystals using the wormlike chain model[17] with a Maier–Saupe pseudopotential.[18,19] This model has been employed by a number of authors to study main-chain liquid crystalline polymers. Warner and coworkers studied both the phase behavior and chain conformation properties in solvent-free systems based on the exact solution of the mean-field equations using spheroidal functions.[14,20] However, the addition of a second component (whether another polymer species or small nonmesogenic solvent) produces new qualitative features in the phase behavior as shown by Liu and Fredrickson.[21,22] In addition, in the approach by Warner and co-workers, the mean-field approximation is introduced as an *ansatz* instead of being derived as the lowest order approximation in a systematic approach. Furthermore, by restricting the interaction to a spatially independent scalar form using the second Legendre polynomial $P_2(\tau)=3u_z^2(\tau)/2-1/2$, the approach can only treat the homogeneous state.

Liu and Fredrickson[21] derived an analytical free energy functional for semiflexible polymer blends using a gradient and order parameter expansion to the quartic order around

 © 2003 American Institute of Physics

Downloaded 14 Dec 2005 to 131.215.225.9. Redistribution subject to AIP license or copyright, see http://jcp.aip.org/jcp/copyright.jsp

the uniform isotropic state. Their approach begins with a field-theoretical formulation of the exact partition function and develops the free energy expansion in a systematic manner. The advantage of the Liu–Fredrickson theory is that it is analytical and convenient for treating inhomogeneous systems.[23] However, its accuracy for describing the nematic state is *a priori* not clear, given the strongly first-order nature of the isotropic–nematic transition. Furthermore, the order parameter expansion uses chain statistics in the isotropic state and thus cannot describe the chain conformation properties in the nematic state.

Other authors used simplified versions of the wormlike chain model which do not conserve the local contour length.[24–27] While such simplified models may capture the qualitative behavior of certain aggregate properties, the chain statistics described by these models are different from that given by the wormlike chain model. They also fail to capture the dynamic properties of a semiflexible chain.[28,29]

In this article, we adapt the exact mean-field solution method of Warner and co-workers to the study of lyotropic systems. We follow the field-theoretical formulation of Liu and Fredrickson, but instead of performing an expansion around the isotropic state, we derive the exact mean-field equations valid for both the isotropic and nematic states, and solve these equations using the spheroidal functions. Our work thus combines the strengths of both approaches. In particular, it provides a nonperturbative description of the thermodynamics and single-chain conformation properties in the nematic state and is amenable to systematic corrections to account for fluctuation effects.

This paper is organized as follows: In Sec: II, we present the model and develop the mean-field equations as the lowest-order approximation to a more systematic approach. The solution method using spheroidal functions is discussed in Sec. III where we also work out the ground-state dominance criteria useful for obtaining a number of analytical results in the long chain limit and explore the asymptotic behavior of some thermodynamic properties in the strong nematic field limit. In Sec. IV, we present the bulk (zero wave number) fluctuation free energy to quadratic order around the mean-field solution in connection to the calculation of the limit of stability (spinodal) of the various phases. In Sec. V we present the main results of the calculation. Several phase diagrams are calculated to illustrate different types of phase behaviors that can result depending on the interplay between the isotropic and anisotropic part of the two-body interaction. By analyzing the shape and location of spinodal curves in these phase diagrams, we propose several interesting scenarios for the phase transition kinetics. The effects of chain stiffness on the nematic order are also briefly discussed in reference to the rigid-rod limit, and we find that small fluctuations of the backbone of the polymers can significantly suppress the emergence of nematic order. We then examine a number of single-chain properties in the nematic state, with an emphasis on the anisotropy of the chain conformation and various energetic contributions. For sufficiently long chains, we provide exact expressions for the longitudinal and transverse correlation lengths in terms of the eigenvalues of the spheroidal functions, which reduce to earlier results by Odijk[30–32] and Tkachenko and Rabin[33] derived in the limit of large nematic field strength. We end this paper with a brief summary and conclusion in Sec. VI.

II. SELF-CONSISTENT-FIELD THEORY

We consider an incompressible system composed of n_p polymer chains and n_s solvent molecules. The polymer molecules are modeled as wormlike chains[17] with cross-sectional area A and fixed contour length L, and the solvent molecules are spherical, nonmesogenic particles with volume v. We work with an open system (grand canonical ensemble) wherein the polymer solution in volume V and at temperature T is connected to an external reservoir; thus the characteristic free energy G of our system is

$$G(V,\mu)=Vg(\mu)=V[f(\phi_p)-\mu\phi_p], \tag{1}$$

where f is the Helmholtz free energy density and μ a chemical potential-like variable that is conjugate to the polymer volume fraction ϕ_p.

The configuration of our system is given by the position and conformation of each polymer molecule and the position of each solvent molecule. The position and conformation of the ith polymer is described by the spacecurve $\boldsymbol{r}_i(\tau)$ where the path coordinate τ runs from zero to L. We define the tangent vector $\boldsymbol{u}_i(\tau)=\partial_\tau \boldsymbol{r}_i(\tau)$ and enforce the fixed polymer length constraint by requiring $|\boldsymbol{u}_i(\tau)|=1$ at all τ. The position of the jth solvent molecule is denoted by $\boldsymbol{r}_j$.

We model the interactions in the system by a local two-body pseudopotential and separate the pseudopotential into isotropic and anisotropic contributions. Thus the Hamiltonian of our system is

$$\beta\mathcal{H}=\sum_{i=1}^{n_p}\frac{\epsilon}{2}\int_0^L\left(\frac{\partial \boldsymbol{u}_i}{\partial\tau}\right)^2 d\tau+\chi\int d\boldsymbol{r}\hat{\phi}_s(\boldsymbol{r})\hat{\phi}_p(\boldsymbol{r}) - \frac{a}{2}\int d\boldsymbol{r}\hat{\mathbf{S}}(\boldsymbol{r}):\hat{\mathbf{S}}(\boldsymbol{r}), \tag{2}$$

where $\hat{\phi}_s$ and $\hat{\phi}_p$, are, respectively, the local dimensionless density (volume fraction) of the solvent and polymer molecules, and $\hat{\mathbf{S}}$ is the tensorial nematic order parameter density (again made dimensionless). They are given by

$$\hat{\phi}_s(\boldsymbol{r})=v\sum_{j=1}^{n_s}\delta(\boldsymbol{r}-\boldsymbol{r}_j), \tag{3}$$

$$\hat{\phi}_p(\boldsymbol{r})=A\sum_{i=1}^{n_p}\int_0^L d\tau\delta(\boldsymbol{r}-\boldsymbol{r}_i(\tau)), \tag{4}$$

$$\hat{\mathbf{S}}(\boldsymbol{r})=A\sum_{i=1}^{n_p}\int_0^L d\tau\delta(\boldsymbol{r}-\boldsymbol{r}_i(\tau))\left(\boldsymbol{u}_i(\tau)\boldsymbol{u}_i(\tau)-\frac{1}{3}\mathbf{I}\right). \tag{5}$$

The first term in the Hamiltonian [Eq. (2)] is the bending energy of the n_p polymer chains, assumed to be quadratic in the curvature of the polymer conformations. The bending modulus ϵ, which has units of length, is equal to the persistence length of the fluctuating chain in the absence of intermolecular interactions. The second term in Eq. (2) is the

Downloaded 14 Dec 2005 to 131.215.225.9. Redistribution subject to AIP license or copyright, see http://jcp.aip.org/jcp/copyright.jsp

isotropic part of the two-body interaction between polymer and solvent molecules, taken to be the Flory–Huggins type.[34] The Flory–Huggins parameter χ contains both an athermal entropic contribution as well as an enthalpic component,[35] thus we may write χ as $\chi=\chi_S+\chi_H/T$. The last term in Eq. (2) is the anisotropic component of the two-body polymer–polymer interaction taken to be of the Maier–Saupe-type,[18,19] which prefers to align the polymer chains within the solution. In general, the Maier–Saupe potential contains both hard-core contact interactions and soft attractive interactions; therefore, we anticipate the Maier–Saupe parameter a, which has units of inverse volume, to have the temperature dependence $a=a_S+a_H/T$.[24] The details of the molecular interactions are simplified by introducing these two phenomenological pseudo-potentials, and the effect of hard-core short-ranged repulsion is accounted for through the incompressibility constraint.

The grand canonical partition function Ξ is found by summing over all system configurations that are consistent with the incompressibility and chain length constraints that we impose on our system; it is given by

$$\Xi=\exp[-\beta G(T,V,\mu)]=\sum_{n_s,n_p=0}^{\infty}\frac{1}{n_s!n_p!}\frac{e^{\beta\mu LAn_p}}{v^{n_s}(LA)^{n_p}}\int\prod_{j=1}^{n_s}d\boldsymbol{r}_j\int\prod_{i=1}^{n_p}\mathcal{D}[\boldsymbol{r}_i]\times\prod_{\boldsymbol{r}}\delta(\hat{\phi}_s+\hat{\phi}_p-1)\prod_{\tau}\delta(|\partial_\tau\boldsymbol{r}_i|-1)e^{-\beta\mathcal{H}}, \tag{6}$$

where $\Pi_{\boldsymbol{r}}\delta(\hat{\phi}_s+\hat{\phi}_p-1)$ accounts for the incompressibility constraint $\hat{\phi}_s+\hat{\phi}_p=1$ at all locations within the system volume, and $\Pi_\tau\delta(|\partial_\tau\boldsymbol{r}_i|-1)$ denotes the fixed chain length constraint $|\partial_\tau\boldsymbol{r}_i|=1$ over the entirety of the path coordinate τ for each polymer chain. The integration over $\mathcal{D}[\boldsymbol{r}_i]$ implies path integration over all conformations of the polymer chain.[36] We use the solvent volume v and polymer volume LA as volume scales instead of the de Broglie wavelengths cubed, which merely shifts the chemical potential by a constant quantity and does not affect the thermodynamic behavior of our system.

The partition function Eq. (6) cannot be evaluated exactly due to the many-chain nature of the molecular interactions and the incompressibility constraint. To make progress, we use field-theoretical techniques[37,38] to transform the many-chain problem into a single-chain problem in fluctuating effective potential fields. This is done by performing a series of identity transformations through functional integration over a number of auxiliary field variables. The resulting expression for the grand canonical partition function is now

$$\Xi=\int\mathcal{D}\phi_p\mathcal{D}W_s\mathcal{D}W_p\mathcal{D}\mathbf{S}\mathcal{D}\boldsymbol{\Lambda}\exp\left\{i\int d\boldsymbol{r}W_s(1-\phi_p)+i\int d\boldsymbol{r}[W_p\phi_p+\boldsymbol{\Lambda}:\mathbf{S}]-\chi\int d\boldsymbol{r}\phi_p(1-\phi_p)+\frac{a}{2}\int d\boldsymbol{r}\mathbf{S}:\mathbf{S}+\frac{1}{v}z_s(W_s)+\frac{e^{\beta\mu LA}}{LA}z_p(W_p,\boldsymbol{\Lambda})\right\}, \tag{7}$$

where ϕ_p and $\mathbf{S}$ are, respectively, the local volume fraction and order parameter density fields, and W_s, W_p, and $\boldsymbol{\Lambda}$ are effective fluctuating fields conjugate to the solvent volume fraction, the polymer volume fraction, and the order parameter density, respectively. The solvent volume fraction has been eliminated by the use of the incompressibility constraint. In Eq. (7), $z_s(W_s)$ and $z_p(W_p,\boldsymbol{\Lambda})$ are, respectively, the single-solvent-molecule partition function and single-polymer-chain partition function, given by

$$z_s(W_s)=\int d\boldsymbol{r}e^{-iv W_s(\boldsymbol{r})} \tag{8}$$

and

$$z_p(W_p,\boldsymbol{\Lambda})=\int\mathcal{D}[\boldsymbol{r}(\tau)]\exp\left\{-\frac{\epsilon}{2}\int_0^L\left(\frac{\partial\boldsymbol{u}}{\partial\tau}\right)^2d\tau-iA\int_0^L d\tau\left[W_p(\boldsymbol{r}(\tau))+\boldsymbol{\Lambda}(\boldsymbol{r}(\tau)):\left(\boldsymbol{uu}-\frac{1}{3}\mathbf{I}\right)\right]\right\}. \tag{9}$$

Though equally difficult to evaluate exactly, the partition function written in the form of Eq. (7) is more amenable to systematic approximations. In particular, the self-consistent-field, or mean-field approximation (we will use these two terms synonymously in this paper), is obtained by a saddle-point approximation to the functional integrals, i.e., by locating the stationary points of the exponent in Eq. (7) with respect to the field variables.

Setting the functional derivatives of the exponent in Eq. (7) with respect to the field variables to zero, we obtain the self-consistent-field equations:

$$1-\phi_p=e^{-vw_s}, \tag{10}$$

$$\phi_p=-\frac{e^{\beta\mu LA}}{LA}\frac{\delta z_p}{\delta w_p}, \tag{11}$$

$$w_p-w_s=\chi(1-2\phi_p), \tag{12}$$

$$\mathbf{h}=-a\mathbf{S}, \tag{13}$$

$$\mathbf{S}=-\frac{e^{\beta\mu LA}}{LA}\frac{\delta z_p}{\delta\mathbf{h}}, \tag{14}$$

where we have defined the fields $w_s=iW_s$, $w_p=iW_p$, and $\mathbf{h}=i\boldsymbol{\Lambda}$ on account of the fact that the saddle-point values of the field variables W_s, W_p, and $\boldsymbol{\Lambda}$ lie on the imaginary axis.

At the mean-field level, the above set of equations fully describe the thermodynamics, and, through the single-chain partition function [Eq. (9)], the conformation properties of the liquid-crystalline polymer solution modeled by the Hamiltonian [Eq. (2)]. They are applicable to problems involving spatial inhomogeneity of polymer concentration and order. Here we focus on the equilibrium, bulk behavior with uniaxial order.

We choose the nematic director to be aligned in the z direction; thus the order parameter is given by

$$\mathbf{S}=S_0(\hat{z}\hat{z}-\tfrac{1}{3}\mathbf{I}). \tag{15}$$

Downloaded 14 Dec 2005 to 131.215.225.9. Redistribution subject to AIP license or copyright, see http://jcp.aip.org/jcp/copyright.jsp

The self-consistent-field equations can be solved analytically by first eliminating the variables, w_s, w_p, and $\mathbf{h}$ in favor of the bulk volume fraction of the polymers, ϕ_p, and the scalar order parameter S_0. Because $\mathbf{S}$ is defined as the order parameter density, S_0 vanishes in the limit of zero concentration even if all the chains are fully aligned. We thus define a normalized scalar order parameter m by

$$m=\frac{S_0}{\phi_p}=\frac{1}{L}\int_0^L d\tau\left\langle\left(\frac{3}{2}u_z^2(\tau)-\frac{1}{2}\right)\right\rangle, \tag{16}$$

where $\langle\cdots\rangle$ indicates an average with respect to the single-chain, self-consistent-field Hamiltonian

$$\beta\mathcal{H}_0=\frac{\epsilon}{2}\int_0^L\left(\frac{\partial\mathbf{u}}{\partial\tau}\right)^2 d\tau-a\phi_p mA\int_0^L d\tau\left(u_z^2(\tau)-\frac{1}{3}\right). \tag{17}$$

We note the effective Hamiltonian [Eq. (17)] only contains orientation terms thus simplifying the calculation of the chain statistics, which we discuss in more detail in the following section.

The grand potential density g is equivalently expressed as the osmotic pressure defined through $p=-[g(\phi_p)-g(0)]$ and given by

$$\beta p=-\frac{1}{v}\log(1-\phi_p)-\chi\phi_p^2-\frac{1}{3}a\phi_p^2m^2-\frac{\phi_p}{v}+\frac{\phi_p}{LA}. \tag{18}$$

The chemical potential μ is given by

$$\beta\mu=\frac{1}{LA}\log\phi_p-\frac{1}{v}\log(1-\phi_p)+\chi(1-2\phi_p)-\frac{1}{LA}\log q, \tag{19}$$

where the single-polymer molecule orientation partition function q is calculated from the self-consistent field Hamiltonian, Eq. (17). And finally, the Helmholtz free energy density (up to an additive constant) for a single, homogeneous phase is

$$\begin{aligned}\beta f&=-\beta p+\beta\mu\phi_p\\&=\frac{\phi_p}{LA}\log\phi_p+\frac{(1-\phi_p)}{v}\log(1-\phi_p)\\&\quad+\chi\phi_p(1-\phi_p)+\frac{a}{3}\phi_p^2m^2\\&\quad+\frac{\phi_p}{v}-\frac{\phi_p}{LA}-\frac{\phi_p}{LA}\log q.\end{aligned} \tag{20}$$

Phase coexistence can be found by minimizing the total Helmholtz free energy of a composite system of two homogeneous phases or equivalently by the respective equality of the osmotic pressure and the chemical potential of the two coexisting phases. In Sec. V, we demonstrate several scenarios for phase separation that are predicted by our model.

Equations (10)–(14) constitute the exact solution for the saddle point of Eq. (7). The solution of the self-consistent Eq. (16) and the evaluation of the single-chain partition function q in Eq. (19) require the conformation statistics of a single chain in a finite nematic field [cf. Eq. (17)]. We address the single chain statistics in Sec. III by mapping it to the quantum mechanics of a rigid rotor in a quadrupole field for which spheroidal functions provide the exact eigenfunctions.

In the solvent-free limit, our results reduce to that previously given by Wang and Warner for thermotropic nematic polymers.[20] Transition from an isotropic phase to a nematic phase occurs when

$$-\log 4\pi=\frac{aLA}{3}m^2-\log q, \tag{21}$$

where m is determined self-consistently from Eq. (16).

III. CHAIN STATISTICS

The self-consistent-field approximation reduces the many-chain problem to a single chain in a (self-consistent) external field. Thus an essential input to the SCF theory is the single-chain statistics. The chain statistics are described by a Green's function $G(\mathbf{r},\mathbf{u}|\mathbf{r}_0,\mathbf{u}_0,L)$, which gives the joint probability for a polymer chain to start and end with specified positions and orientations as a function of the chain length. While in general we need to consider both the position and orientation dependence of the Green's function, for the homogeneous phases we consider here, it suffices to focus on the orientation variable. Thus we consider the reduced Green's function $G(\mathbf{u}|\mathbf{u}_0,L)$, defined as

$$G(\mathbf{u}|\mathbf{u}_0,L)=\int_{\mathbf{u}_0}^{\mathbf{u}}\mathcal{D}[\mathbf{u}(\tau)]e^{-\beta\mathcal{H}_0[\mathbf{u}(\tau)]}, \tag{22}$$

from which the partition function q and the order parameter m can be calculated using

$$q=\int d\mathbf{u}\int d\mathbf{u}_0 G(\mathbf{u}|\mathbf{u}_0,L), \tag{23}$$

$$m=\frac{3}{2L}\left(\frac{\partial\log q}{\partial\kappa}\right)_{\epsilon}, \tag{24}$$

where $\kappa=a\phi_p mA$.

The orientation path integration for the Green's function of a wormlike chain is analogous to the calculation of the probability amplitude for a quantum mechanical rotor, where the chain length plays the role of an imaginary time variable.[36,39] Using this analogy, we derive a diffusion equation for the chain statistics that is analogous to the Schrödinger equation. The diffusion equation for the Green's function is

$$\left[\frac{\partial}{\partial L}-\frac{1}{2\epsilon}\nabla_u^2-a\phi_p mA\left(u_zu_z-\frac{1}{3}\right)\right]G(\mathbf{u}|\mathbf{u}_0,L)=\delta(L)\delta(\mathbf{u}-\mathbf{u}_0), \tag{25}$$

where ∇_u^2 is the angular portion of the Laplace operator. Our statistical problem is essentially a unit vector diffusing over the surface of a sphere, biased by a quadrupole potential favoring the poles.

Downloaded 14 Dec 2005 to 131.215.225.9. Redistribution subject to AIP license or copyright, see http://jcp.aip.org/jcp/copyright.jsp

Equation (25) is solved using an eigenfunction expansion by defining the Hamiltonian operator $\mathcal{H}=-\nabla_u^2-\gamma u_z u_z$, where $\gamma=2a\phi_p\epsilon mA=2\epsilon\kappa$. The eigenfunctions of $\mathcal{H}$ are the spheroidal functions[40] Ysp_l^m with eigenvalues $\mathcal{E}_l^m(\gamma)$. Owing to the completeness of the spheroidal functions, the Green's function is written as

$$G(\mathbf{u}|\mathbf{u}_0,L)=\sum_{l=0}^{\infty}\sum_{m=-l}^{l}C_l^m(L)Ysp_l^m(\mathbf{u})Ysp_l^{m*}(\mathbf{u}_0), \quad (26)$$

accounting for the initial condition $G(\mathbf{u}|\mathbf{u}_0,0)=\delta(\mathbf{u}-\mathbf{u}_0)$, where the chain-length dependent coefficients are given by

$$C_l^m=\exp\left[-\left(\mathcal{E}_l^m(\gamma)+\frac{\gamma}{3}\right)\frac{L}{2\epsilon}\right]. \quad (27)$$

Since the Green's function only provides orientation statistics, the expectation value of any quantity must be expressed in terms of orientation variables only. Clearly the Green's function including position variables provides an easier formalism for calculating arbitrary averages; however, analytical expressions for the full Green's function do not exist, and approximate techniques have a limited range of validity.[39]

Several methods exist for the calculation of the spheroidal functions. Numerical packages[41–43] have been developed that accurately evaluate the functions and their eigenvalues. The spheroidal functions can also be evaluated by expansion in terms of the more common spherical harmonics (Y_l^m);[20,40] we outline this technique in Appendix A. The spheroidal functions asymptotically approach the spherical harmonics in the limit of $\gamma\to 0$, thus in this limit, $\mathcal{E}_l^m$ approaches $l(l+1)$. The opposite limit ($\gamma\to\infty$) yields asymptotic expressions for $\mathcal{E}_l^m$ in terms of γ,[40] which we exploit later in this section.

While the eigenfunction expansion Eq. (26) is formally exact for any bending rigidity, the limit of a fully rigid chain ($\epsilon\to\infty$) is more conveniently solved directly by setting $\epsilon\to\infty$ in Eq. (25), which yields

$$G(\mathbf{u}|\mathbf{u}_0,L)=\exp\left[a\phi_p mAL\left(u_z^2-\frac{1}{3}\right)\right]\delta(\mathbf{u}-\mathbf{u}_0). \quad (28)$$

The partition function in this limit is

$$q=4\pi h^{-1}\exp\left(-\frac{h^2}{3}\right)\int_0^h dx\exp(x^2),$$

$$=2\pi^{3/2}h^{-1}\exp\left(-\frac{h^2}{3}\right)\mathrm{erf}(ih), \quad (29)$$

where $h=\sqrt{a\phi_p mAL}$ and erf is the error function. The order parameter is given by

$$m=\frac{3\pi\exp\left(\frac{2}{3}h^2\right)}{h^2 q}-\frac{3}{4h^2}-\frac{1}{2}. \quad (30)$$

The expression for the partition function requires evaluation of the parameter h by solving the self-consistent equation for the order parameter. The rigid rod limit provides an important reference for examining the effects of finite chain flexibility, which we discuss in Sec. V.

Since the rigid rod limit represents the limit where all eigenfunctions are necessary in the Green's function to properly capture the chain statistics, the opposite limit occurs when only a couple of eigenfunctions need to be included in the Green's function, which we define as the limit of ground-state dominance.[20,44] This typically occurs for long chain length; however, the behavior of the arguments of C_l^m within Eq. (26) in the presence of the nematic interaction alters the criteria for ground-state dominance. Furthermore, the number of eigenfunctions required to capture the chain statistics depends on the field strength; for example, the isotropic state requires only the ground state, whereas it is necessary to include both the ground and first excited states to capture the chain statistics in the limit of strong field strength. Therefore, for arbitrary field strength γ, we identify the general criteria for ground-state dominance as

$$\frac{L(\mathcal{E}_2^0-\mathcal{E}_0^0)}{2\epsilon}\gg 1, \quad (31)$$

requiring a large separation between the ground and second excited states. We determine the ground-state dominance criteria analytically for the limit of weak and strong field strength.

As previously stated, the eigenvalues $\mathcal{E}_l^m$ approach $l(l+1)$ as γ goes to zero (weak nematic interaction). In this limit, ground-state dominance occurs when $L/\epsilon\gg 1$. The Green's function is dominated by the first term only, which has a trivial behavior since $Ysp_0^0\to 1/\sqrt{4\pi}$ in this limit (independent of orientation); the effect of the chain rigidity is only significant when the chain length is comparable in size to the persistence length.

The case of strong nematic interaction ($\gamma\gg 1$) presents a very different scenario. In this limit, adjacent eigenvalues of the spheroidal functions asymptotically approach each other, i.e., $\mathcal{E}_{m+2n+1}^m\to\mathcal{E}_{m+2n}^m$ ($n=0,1,2,...$) as $\gamma\to\infty$; therefore, the coefficient of the ground and first excited states asymptotically approach each other in Eq. (26) ($C_0^0\to C_1^0$). We must include both the ground and first excited states in this limit in order to properly capture the chain statistics. Criteria for ground-state dominance [Eq. (31)] requires a large separation between the nearly degenerate ground states and the next excited state. Using the asymptotic behavior of $\mathcal{E}_l^m$ for $\gamma\gg 1$,[40] this occurs when

$$\frac{L}{2\epsilon}\left[4\gamma^{1/2}-4-\frac{7}{2\gamma^{1/2}}+\mathcal{O}(\gamma^{-1})\right]\gg 1. \quad (32)$$

Ground-state dominance thus occurs for a combination of long polymer chains and/or large interaction strength. Unlike the case of ground-state dominance for weak interaction, the Green's function in this limit demonstrates very rich physical behavior, which we explore in Sec. V.

Here we provide the asymptotic expressions for the single-chain partition function and the normalized nematic order parameter that appear in the SCF equations in the limit of $\gamma\gg 1$. Keeping all available terms

Downloaded 14 Dec 2005 to 131.215.225.9. Redistribution subject to AIP license or copyright, see http://jcp.aip.org/jcp/copyright.jsp

$$\log q = \frac{L}{2\epsilon}\left(\frac{2}{3}\gamma - 2\gamma^{1/2} + 1 + \frac{1}{4\gamma^{1/2}} + \frac{1}{4\gamma} + \frac{23}{64\gamma^{3/2}} + \frac{41}{64\gamma^2} + \frac{681}{512\gamma^{5/2}} + \mathcal{O}(\gamma^{-3})\right), \tag{33}$$

$$m = 1 - \frac{3}{2\gamma^{1/2}} - \frac{3}{16\gamma^{3/2}} - \frac{3}{8\gamma^2} - \frac{207}{256\gamma^{5/2}} - \frac{123}{64\gamma^3} - \frac{10\,215}{2048\gamma^{7/2}} - \mathcal{O}(\gamma^{-4}). \tag{34}$$

As in the rigid limit, Eq. (34) provides a self-consistent equation for solving for the order parameter m, or equivalently the interaction strength γ, which is then used in the expression for q. We define the single-chain quadrupole (i.e., second Legendre polynomial P_2) fluctuation as

$$\Delta_m = \frac{1}{L^2}\int_0^L d\tau \int_0^L d\tau' \langle P_2(\tau) P_2(\tau')\rangle - \left(\frac{1}{L}\int_0^L d\tau \langle P_2(\tau)\rangle\right)^2 = \frac{9}{4L^2}\left(\frac{\partial^2 \log q}{\partial \kappa^2}\right)_\epsilon, \tag{35}$$

which we make use of in Sec. IV. The asymptotic behavior of Δ_m is given by

$$\Delta_m = \frac{9\epsilon}{4L}\left(\frac{1}{\gamma^{3/2}} + \frac{3}{8\gamma^{5/2}} + \frac{1}{\gamma^3} + \frac{345}{128\gamma^{7/2}} + \frac{123}{16\gamma^4} + \frac{23\,835}{1024\gamma^{9/2}} + \mathcal{O}(\gamma^{-5})\right). \tag{36}$$

The asymptotic behavior for q, m, and Δ_m permits the evaluation of the binodal and spinodal curves in the limit defined by Eq. (31).

In the flexible chain limit ($\epsilon/L \to 0$), the spheroidal functions become the spherical harmonics; therefore, the use of Eq. (26) in the flexible limit provides analytical expressions for chain averages. The flexible limit results in a solution with no orientational order ($m=0$); however, the quadrupole fluctuation Δ_m has a finite value,[21] which is given by

$$\Delta_m = \frac{6\epsilon}{45L}\left\{1 - \frac{\epsilon}{3L}\left[1 - \exp\left(-\frac{3L}{\epsilon}\right)\right]\right\}. \tag{37}$$

With this expression, the limit of metastability of the isotropic phase can be calculated using the equations provided in Sec. IV.

IV. GAUSSIAN FLUCTUATIONS

Our development of the SCF theory provides a natural framework for incorporating fluctuations. This is accomplished by including fluctuations in the field variables from their saddle-point or SCF values. Of particular interest is the free energy cost for arbitrary density and order parameter fluctuations in the nematic state. Such a free energy yields information on the concentration–concentration, order-parameter–order-parameter, and concentration–order-parameter correlations, as well as the thermodynamic stability of the system. When properly projected, the fluctuation free energy in the nematic state can be used to determine the three Frank elastic constants[45] for the long wavelength bending, splay and twist deformation of the nematic director. This idea has been used in the work of Liu and Fredrickson.[21] However, as alluded to in the introduction, their treatment of the nematic state is through an order-parameter expansion around the isotropic state which makes use of chain statistics in the isotropic state. Not only is the description of the nematic state approximate, but the chain conformation change as described in Sec. V and its influence on the thermodynamics cannot be properly captured in this perturbative approach. In contrast, our theory will treat fluctuations around the exact saddle point; the chain conformation changes and the attended changes in thermodynamics will be automatically incorporated through the single-chain partition function in the self-consistent field.

We defer the presentation of the general fluctuation theory to a future paper. In this paper, we restrict our consideration to homogeneous, or zero-wavenumber fluctuations in the density and the magnitude of the order-parameter to illustrate the main idea. The spinodal, or limit of metastability, is determined from the vanishing of the determinant of the quadratic coefficients of the fluctuation free energy.

Starting from our expression for Ξ in terms of the functional integral [Eq. (7)], we write the field variables as their saddle-point values plus fluctuations, and expand the exponent in the integrand to quadratic order in the fluctuations. The linear terms vanish identically owing to the saddle-point nature of the expansion. The quadratic fluctuations in the auxilliary fields ΔW_s, ΔW_p, and $\Delta\Lambda$ can be easily integrated out to yield a resulting fluctuation free energy in terms of the fluctuation in the physical fields: The density $\Delta\phi_p$ and the order-parameter ΔS. The fluctuation free energy is

$$\frac{\beta\Delta G}{V} = \frac{1}{2}\left(\frac{1}{v(1-\phi_p)} + \frac{1}{LA\phi_p} + \frac{m^2}{LA\phi_p\Delta_m} - 2\chi\right)\times\Delta\phi_p\Delta\phi_p - \frac{m}{LA\phi_p\Delta_m}\Delta\phi_p\Delta S + \frac{1}{2}\left(\frac{1}{LA\phi_p\Delta_m} - \frac{2a}{3}\right)\Delta S\Delta S \equiv \frac{C_{\phi\phi}}{2}\Delta\phi_p\Delta\phi_p + C_{\phi S}\Delta\phi_p\Delta S + \frac{C_{SS}}{2}\Delta S\Delta S. \tag{38}$$

We use Eq. (38) to determine the limit of metastability, or spinodal, of a homogeneous phase, either isotropic or nematic. Instability occurs when fluctuations reduce the free energy. In the case of an isotropic phase, the order-parameter and concentration fluctuations are uncoupled; thus the spinodal occurs when either C_{SS} or $C_{\phi\phi}$ is equal to zero, the former corresponding to an instability with respect to the nematic state and the latter corresponding to isotropic–isotropic phase separation. For the nematic case, we see that the modes are coupled in the fluctuation free energy; there-

Downloaded 14 Dec 2005 to 131.215.225.9. Redistribution subject to AIP license or copyright, see http://jcp.aip.org/jcp/copyright.jsp

fore, instability occurs by a mixture of concentration and order-parameter fluctuations, marked by the vanishing of the determinant of C_{ij} $(i,j=\phi_p,S)$.

We note that, perhaps to be expected, the spinodals identified from examining the fluctuation around the saddle point coincide with those determined from the matrix of the second derivatives of the Helmholtz free energy. However, the free energy cost for fluctuations around the saddle point can only be correctly calculated by the fluctuation free energy described here.

V. RESULTS AND DISCUSSION

With the self-consistent-field theory, we can address both the phase behavior and the chain statistics at the mean-field level. We first define the set of dimensionless parameters that will be used in the calculations presented in this section. Since the volume of the solvent v enters as a natural volume scale, we define a dimensionless volume of the polymer N by $N=LA/v$, which can be considered an effective degree of polymerization. The Maier–Saupe and Flory–Huggins parameters, both having dimensions of inverse volume, can be similarly made dimensionless by defining $\tilde{a}=av$ and $\tilde{\chi}=\chi v$. A dimensionless persistence length (or bending energy) can be defined by $\tilde{\epsilon}=\epsilon A/v$; thus, $N/\tilde{\epsilon}=L/\epsilon$. In the interest of simplifying notation, we will drop the tilde from these dimensionless parameters.

A. Phase behavior

We start with a discussion of the phase behavior of a semiflexible polymer solution. In addition to the coexistence curves between thermodynamically stable phases, we are also interested in determining the various spinodals for the limit of metastable states. Both pieces of information can be obtained from examining the behavior of the grand free energy density (the negative of the osmotic pressure p up to a constant) and the chemical potential μ. A typical plot of these two quantities that shows coexistence and spinodal is given in Fig. 1 for a fixed set of parameter values ($N=20$, $\epsilon=a=3.7875$, and $\chi=1.0100$). We now discuss its key features.

In Fig. 1, we denote the isotropic branch by the solid line and the nematic branch by the dashed line. For low polymer volume fractions, the osmotic pressure is low and the chemical potential is large and negative; the system is a dilute isotropic solution. On the scale of the figure this dilute solution behavior is represented by the nearly vertical line. This line intersects the line representing the concentrated isotropic solution ($\phi_p=\partial p/\partial\mu$) at the point indicated by the diamond. This is the coexistence between a polymer-lean isotropic phase ($\phi_p=0.0030$) and a polymer-rich isotropic phase ($\phi_p=0.6404$). This transition is caused by the positive (repulsive) Flory–Huggins parameter between the solvent and the polymer and is identical to phase separation of flexible polymer solutions at the mean-field level. The segment between the diamond and the asterisk represents a metastable (supersaturated) polymer-lean solution. The asterisk with $\phi_p=0.0518$ marks the limit of metastability. Similarly, the segment between the diamond and the pentagram corresponds to a metastable (undersaturated) polymer-rich phase,

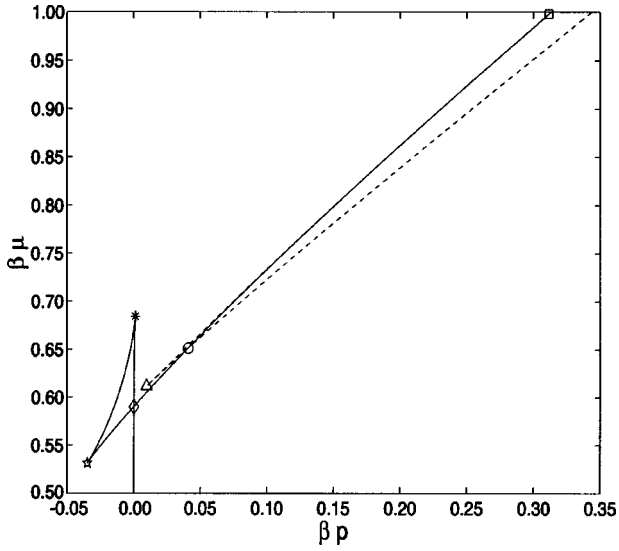

FIG. 1. The solution for the phase behavior for $N=20$, $a=\epsilon=3.7875$, and $\chi=1.0100$ is indicated in this plot of βp vs $\beta\mu$. The nematic branch (dashed line) approaches the isotropic branch (solid line) as the field strength approaches zero. The point of isotropic–nematic coexistence (circle) occurs when the two branches cross. The points of instability associated with this phase transition occur at the triangle and the square. The point of isotropic–isotropic coexistence (diamond) corresponds to the Flory–Huggins phase transition (Ref. 34), and the limits of metastability associated with this phase transition are indicated by the asterisk and the pentagram.

the limit of metastability occuring at the pentagram with $\phi_p=0.4779$. The segment between the pentagram and the asterisk corresponds to thermodynamically unstable states; a system having an overall composition in this range will spontaneously phase separate into the thermodynamically stable polymer-rich and polymer-lean phases with their equilibrium compositions.

For overall volume fractions above $\phi_p=0.6404$, the isotropic branch of the polymer-rich phase crosses the nematic branch at the point indicated by the circle. At this point, the isotropic phase, with a volume fraction of $\phi_p=0.6966$, is in coexistence with a nematic phase, with a volume fraction of $\phi_p=0.8082$. The transition from isotropic to nematic is associated with a first-order jump in the order parameter from zero to $m=0.4711$ for the chosen set of parameters. To the right of the circle, the thermodynamically stable state is the nematic phase. However, the isotropic phase can remain metastable for volume fractions up to $\phi_p=0.8371$ indicated by the square in Fig. 1, where the isotropic phase reaches its spinodal with respect to the nematic state. An interesting characteristic of this instability is that the volume fraction of the isotropic phase at the spinodal is larger than the volume fraction of the nematic phase at the binodal. Consequently, we expect that the metastable isotropic phase will transition directly into a pure nematic phase rather than phase separate into coexisting isotropic and nematic phases. On the nematic branch, in the direction of decreasing the polymer volume fraction, the nematic state becomes metastable below the coexistence volume fraction, $\phi_p=0.8082$. The metastable state terminates at the spinodal point of $\phi_p=0.7589$, indicated by the triangle. As discussed in Sec. IV, the instability of the

Downloaded 14 Dec 2005 to 131.215.225.9. Redistribution subject to AIP license or copyright, see http://jcp.aip.org/jcp/copyright.jsp

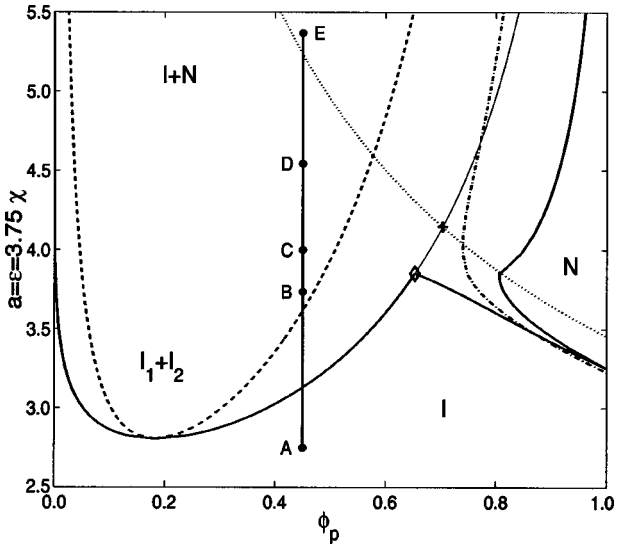

FIG. 2. A phase diagram for a polymer-solvent system with polymer molecules with degree of polymerization $N=20$ for parameter values of $a=\epsilon=3.75\chi$. The solid lines are the binodal coexistence curves. The dashed line is the isotropic spinodal curve due to concentration fluctuations, and the dotted line is the isotropic spinodal curve due to order fluctuations. The dashed–dotted line is the nematic phase spinodal curve, which occurs due to a combination of concentration and order fluctuations. The equilibrium phase behavior is labeled within each region. We label several points of significance that are explained further in the text.

nematic state is due to a combination of concentration and order-parameter fluctuation.

Performing the analysis discussed above as we vary the parameters of the model allows us to construct the phase diagram in these parameters. The interplay between the isotropic Flory–Huggins interaction and the nematic Maier–Saupe interaction, and the different combinations of the enthalpic and entropic contributions in these parameters, can lead to different types of equilibrium phase diagrams. Phase diagrams of our current system, as well as closely related systems, have been found with similar topology as the diagrams that we present in this section.[22,46,47] Assuming a given temperature dependence of the parameters in the model, these phase diagrams can be reproduced more accurately with our current SCF method. However, rather than an exhaustive listing of the types of phase diagrams, we will only discuss three phase diagrams, as examples of the application of our SCF method and to discuss certain issues not emphasized in previous studies.

In the first example, we show a full phase diagram (Fig. 2) for a fixed length of polymer chains $N=20$ over a range of the other parameters ($a=\epsilon=3.75\chi$). When these parameters are purely energetic in origin, increasing them is equivalent to decreasing the temperature. In general, however, χ and a contain both entropic and enthalpic components; thus varying them with the fixed ratio should be more properly interpreted as specifying a particular surface in the larger multidimensional phase diagram. The features we will discuss are not affected by how these parameters are to be interpreted, but for convenience, we will refer to the increase in these interaction parameters as decreasing the temperature.

The equilibrium coexistence curves for the different phases labeled in Fig. 2 are shown by the thick solid lines. As the values of these interaction parameters increase from zero, the first point of significance in Fig. 2 is a critical point at $\chi=0.7486$ and $\phi_p=0.1829$ indicating the beginning of a two-phase region of the phase diagram where a polymer-lean isotropic phase is in coexistence with a polymer-rich isotropic phase. This point corresponds to the critical point predicted in the Flory–Huggins theory,[34] which at the mean-field level is unaffected by the alignment interaction and the bending rigidity. The second point of interest is the onset of nematic ordering in the solvent-free limit ($\phi_p=1$), which occurs at $a=\epsilon=3.2528$ where the order parameter jumps from zero to $m=0.3488$. When solvent is present, the first-order transition in the order parameter is accompanied by a finite concentration change between the isotropic and nematic phases. The isotropic–isotropic coexistence and the isotropic–nematic coexistence meet at a triple point (indicated by the diamond) for $\chi=1.0271$ and $a=\epsilon=3.8515$ where three phases coexist [isotropic 1 ($\phi_p=0.0024$), isotropic 2 ($\phi_p=0.6530$), and nematic ($\phi_p=0.8055$)]. Above the triple point, the thermodynamically preferred phase behavior within the binodal envelope is a polymer-lean isotropic phase in coexistence with a polymer-rich nematic phase.

Of particular interest are the various spinodal lines in the phase diagram. Examination of the location of these spinodals reveals interesting mechanisms for the possible kinetics of the phase changes. Consider, for example, a temperature quench along the vertical bar at $\phi_p=0.45$ in Fig. 2 from the isotropic phase (point A) to a point inside the dashed spinodal. If the quench is to a temperature higher than the triple point (point B), then the system will undergo spinodal decomposition into a polymer-lean isotropic phase and a polymer-rich isotropic phase. However, if the quench is deeper than the triple point, the situation is quite subtle. The reason is that the polymer-rich isotropic branch of the binodal (shown by the thin solid line), though superseded by the nematic branch, never loses its local thermodynamic stability. As long as the concentration of the (isotropic) polymer-rich phase is still below the spinodal with respect to the nematic state shown by the dotted line, it can exist as a metastable state. Thus it is conceivable that for quenches slightly above the triple-point but less than indicated by the cross (point C), the first step in the phase separation is still spinodal decomposition into a polymer-lean isotropic phase and a polymer-rich isotropic phase. The appearance of the nematic phase will take place inside the polymer-rich phase via nucleation. For quenches beyond the cross (point D), the concentration of the polymer in the polymer-rich phase that results from the spinodal decomposition exceeds the spinodal for appearance of the nematic phase; thus as soon as the system phase separates in concentration, the nematic phase will appear spontaneously in the polymer-rich phase. Finally, for very deep quenches beyond the spinodal with respect to the nematic phase (point E), nematic order will appear directly, driving the phase separation into a polymer-lean isotropic phase and a polymer-rich nematic phase. In practice, the last two phase separation scenarios may not be distinguishable, although the primary driving forces are different.

The spinodals to the right of the triple point similarly

Downloaded 14 Dec 2005 to 131.215.225.9. Redistribution subject to AIP license or copyright, see http://jcp.aip.org/jcp/copyright.jsp

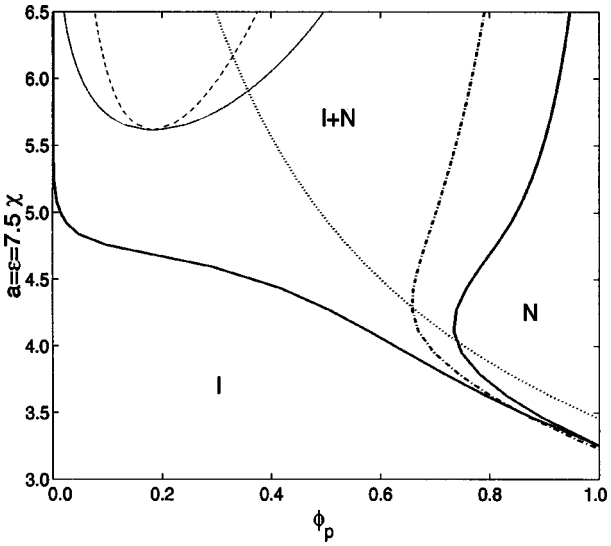

FIG. 3. A phase diagram for a polymer–solvent system with polymer molecules with degree of polymerization $N=20$ for parameter values of $a=\epsilon=7.5\chi$. The solid lines are the binodal coexistence curves. The dashed line is the isotropic spinodal curve due to concentration fluctuations, the dotted line is the isotropic spinodal due to order fluctuations, and the dashed–dotted line is the nematic phase spinodal curve. The equilibrium phase behavior is labeled within each region.

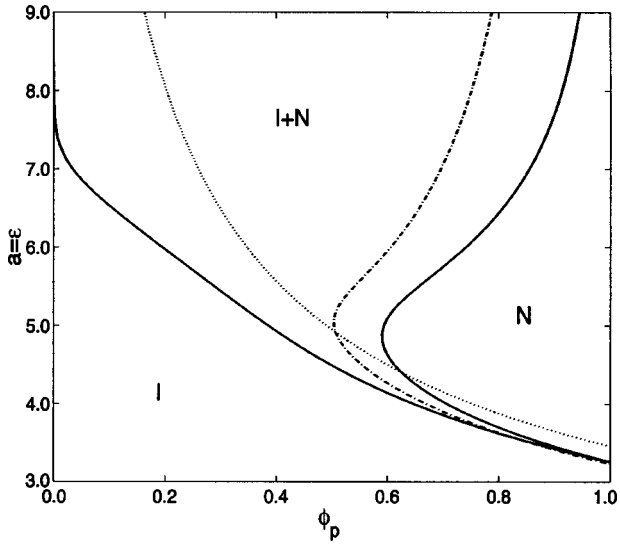

FIG. 4. A phase diagram for a polymer–solvent system with polymer molecules with degree of polymerization $N=20$ for parameter values of $a=\epsilon$ and $\chi=0$. The solid lines are the binodal coexistence curves. The dotted line is the isotropic spinodal curve, and the dashed–dotted line is the nematic phase spinodal curve. The equilibrium phase behavior is labeled within each region.

have interesting kinetic implications. In particular, part of the spinodal of the isotropic polymer-rich phase with respect to nematic ordering lies within the two-phase coexistence region and part of it lies in the single-phase nematic region. Thus, for example, a quench at say $\phi_p=0.7$ beyond this spinodal will lead to phase separation into a polymer-lean isotropic phase and a polymer-rich nematic phase, whereas a quench at $\phi_p=0.9$ will lead to the spontaneous appearance of the nematic order without any phase separation. The kinetic scenario for the latter case is likely the coarsening of nematic domains via nonconserved order parameter dynamics.

The dynamics of spinodal decomposition in a liquid crystal (rodlike)–polymer system[46] is shown to exhibit fibrillar network morphologies in similar scenarios of decomposition as described here. These findings suggest that domain morphology during phase separation is strongly influenced by the quench on the phase diagram as well as the phase separation and ordering kinetics.

As we decrease the Flory–Huggins parameter relative to the Maier–Saupe interaction, the isotropic–isotropic bulge in the phase diagram will shrink, eventually shifting the critical point inside the isotropic–nematic envelope, thus making it a metastable critical point. Figure 3 shows such a phase diagram for a system with $N=20$ and $a=\epsilon=7.5\chi$ (similar parameters as for Fig. 2 with a reduced χ-parameter). Metastable critical points occur in a number of physical systems. In model colloidal systems, for example, when the coexistence curve between two fluid phases lies within the phase envelope between a dilute fluid phase and a crystalline phase, the presence of the metastable critical point is shown to have a dramatic effect on the nucleation barrier for the formation of the crystalline phase.[48,49] In the vicinity of the critical point, the free-energy barrier is dramatically decreased, and nucleation rates increase by many orders of magnitude. Critical fluctuation in the colloidal density creates a locally dense fluid pocket which facilitates the formation of the crystalline phase. It has also been suggested that polymer crystallization from the melt can be similarly assisted by the presence of a buried fluid–fluid binodal curve within the fluid–crystal coexistence envelope, where the nucleation barrier also goes through a minimum at the metastable critical point.[50] The enhancement of crystal nucleation due to the presence of a metastable critical point has important implications in protein and polymer crystallization, where the quality of the final crystalline material is dramatically influenced by the nature of the crystallization process. Because the phase diagram shown in Fig. 3 has identical topology to those for the systems just mentioned, we expect phenomenologically similar effects on nucleation of the nematic phase due to the presence of a metastable isotropic–isotropic critical point.

To complete our discussion of the effect of reduced Flory–Huggins parameter on the phase behavior, we show in Fig. 4 a phase diagram for the limiting case of $\chi=0$, keeping other parameters to be the same as in Figs. 2 and 3. In this case, the isotropic–isotropic coexistence has completely disappeared and the driving force for phase separation is entirely due to the Maier–Saupe alignment interaction. Nevertheless, the energy gain for chains to locally align with each other creates an effective attraction between the chain segments, leading to a large fractionation in the chain density between the isotropic phase and the nematic phase.

The three phase diagrams presented in this article are essentially snapshots of the full phase diagrams along some particular coordinate in the parameter space. Many other types of phase diagrams are possible. For example, for systems where chain alignment is caused by hard-core repulsion, the isotropic part of the chain–chain interaction is re-

Downloaded 14 Dec 2005 to 131.215.225.9. Redistribution subject to AIP license or copyright, see http://jcp.aip.org/jcp/copyright.jsp

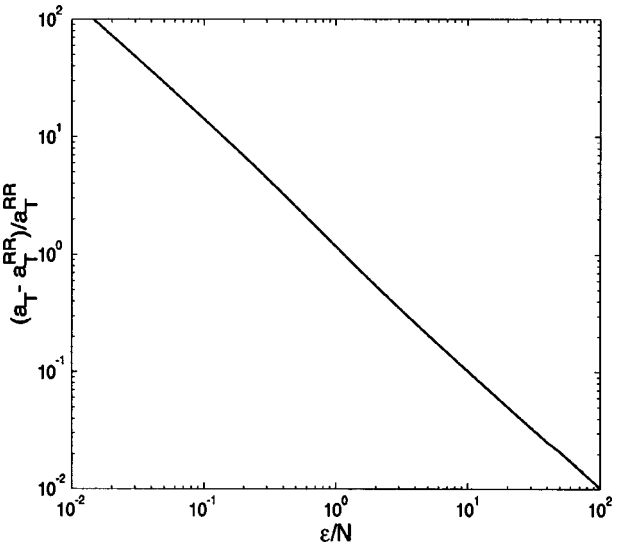

FIG. 5. The behavior of the Maier–Saupe parameter at the thermotropic transition point a_T relative to the rigid rod value vs the reduced chain rigidity ϵ/N for a chain length of $N=20$.

pulsive, leading to a negative χ parameter. The phase diagram that results from this case then resembles that of the Onsager-type[51] for the hard rods with a narrow concentration gap between the isotropic and nematic phases.

We end this section on the phase behavior with a brief discussion of the effects of chain rigidity. Depending on the ratio between the persistence length and the contour length, a wormlike chain is broadly categorized into three scaling regimes: Flexible when this ratio is small, rigid when this ratio is large, and semiflexible when this ratio is of order unity. An interesting question is to what extent can a wormlike chain with large but finite stiffness be described as an effective rigid rod with regard to the phase behavior. To address this question, we have computed several phase diagrams by varying the chain stiffness while keeping other parameters fixed. Instead of showing more phase diagrams, in this article we focus on the value of the Maier–Saupe parameter a_T at the thermotropic ($\phi_p=1$) isotropic–nematic transition, which is governed by Eq. (21). This information is implicitly included in most theoretical studies on the isotropic–nematic transition in wormlike polymers, but we are not aware of any efforts at explicitly addressing the effect of chain stiffness in reference to the rigid limit.

Using Eqs. (29) and (30), we find, for a rigid rod system, the thermotropic isotropic–nematic transition occurs at $a_T^{RR}=6.8122/N$ (the superscript *RR* denotes rigid rod) where the order parameter transitions from zero to $m^{RR}=0.4290$. Since fluctuation from the perfectly straight conformation reduces the degree of orientational order, the onset of nematic order requires a larger Maier–Saupe parameter (or lower temperature) when the bending rigidity is reduced. We plot in Fig. 5 the deviation of a_T from a_T^{RR} $[(a_T-a_T^{RR})/a_T^{RR}]$ over a range of bending rigidity for a fixed chain length $N=20$, found by solving Eq. (21). Figure 5 covers the transition behavior over several orders of magnitude of the reduced chain rigidity ϵ/N thus providing data for polymer systems ranging from very flexible to very rigid. Even for relatively rigid polymer chains, the difference from the perfectly rigid rod transition is substantial. For example, when $\epsilon/N\approx 10$, we see the rigid rod prediction for a_T, and thus the isotropic–nematic transition temperature, is inaccurate by $\sim$10%. This substantial inaccuracy suggests that the range of validity of the rigid rod approximation is quite limited, thus demonstrating the need to consider the finite flexibility for predicting the isotropic–nematic transition in experimental systems.

B. Chain statistics

In this section, we consider the single-chain conformation and thermodynamic properties in a nematic field. At the self-consistent-field level, the single-chain behavior is described by a wormlike chain in a quadrupole potential field of strength $\kappa=a\phi_p mA$; see Eq. (17). Note that since several different combinations of the Maier–Saupe parameter a, the volume fraction of the polymer ϕ_p and the normalized order-parameter m can give the same κ, the single-chain behavior at the SCF level does not correspond to a unique thermodynamic state.

We start with mean-square end-to-end distance tensor given by

$$\langle R_i R_j\rangle = \int_0^L d\tau_1 \int_0^L d\tau_2 \langle u_i(\tau_1) u_j(\tau_2)\rangle, \tag{39}$$

where R_i $(i=1,2,3)$ is the ith component of the end-to-end vector $\boldsymbol{R}\equiv\boldsymbol{r}(L)-\boldsymbol{r}(0)$ of the polymer and we choose the 3rd direction to be that of the nematic director. Evaluation of Eq. (39) is accomplished by calculating the thermal average using the Green's function provided in Sec. III or, alternatively, using the perturbation partition function method given in Appendix B. Since the perturbation partition function is a generator of arbitrary moments of $\boldsymbol{R}$, it can be used to numerically solve for the Green's function that includes the end locations by performing a moment-based expansion;[39] we will not pursue such an effort in this work, however.

In the limit of zero field strength κ, the Hamiltonian Eq. (17) is invariant under arbitrary rotation of the coordinate frame; therefore, the average end-to-end distance is equivalent in all three directions, and symmetry dictates that $\langle R_i R_j\rangle=0$ for $i\neq j$. In this limit, the polymer chain end-to-end behavior is

$$\langle R_i R_j\rangle = \frac{2}{3}\delta_{ij}\left[\epsilon L+\epsilon^2\exp\left(-\frac{L}{\epsilon}\right)-\epsilon^2\right], \tag{40}$$

where δ_{ij} is the Kronecker delta. Equation (40) has the ballistic scaling L^2 for $L/\epsilon\ll 1$ and the diffusive scaling L for $L/\epsilon\gg 1$, signifying the cross-over from a relatively rigid to a relatively flexible polymer chain. The chain statistics identify the persistence length ϵ as an orientation correlation length.

For finite values of the field strength κ, the arbitrary rotational invariance of the Hamiltonian is broken. However, Eq. (17) is invariant under rotation about the z axis (third direction). The chain statistics for the Hamiltonian results in $\langle R_1^2\rangle=\langle R_2^2\rangle\neq\langle R_3^2\rangle$, and symmetry dictates that $\langle R_i R_j\rangle=0$ for $i\neq j$. The splitting of the average end-to-end distance in the directions perpendicular (transverse) to the nematic field (1 and 2) from the parallel (longitudinal) direction (3) im-

Downloaded 14 Dec 2005 to 131.215.225.9. Redistribution subject to AIP license or copyright, see http://jcp.aip.org/jcp/copyright.jsp

plies the emergence of two different orientation correlation lengths: The transverse correlation length $\xi_\perp$ and the longitudinal correlation length $\xi_\parallel$. Due to the favorable interaction between the chain tangent vector and the nematic field, we expect $\xi_\parallel > \xi_\perp$.

The average $\langle R_i R_j \rangle$ can be readily evaluated numerically using the eigenfunction expansion of the Green's function. However, ground-state dominance is valid over a wide range of parameter values (criteria discussed in Sec. III) and is useful in predicting the behavior of $\xi_\perp$ and $\xi_\parallel$. Evaluation of $\langle u_i(\tau_1) u_j(\tau_j) \rangle$ is greatly simplified for the case of ground-state dominance, and we find

$$\xi_\perp = \frac{2\epsilon}{\mathcal{E}_1^1 - \mathcal{E}_0^0}, \tag{41}$$

$$\xi_\parallel = \frac{2\epsilon}{\mathcal{E}_1^0 - \mathcal{E}_0^0}. \tag{42}$$

Equations (41) and (42) are valid for arbitrary values of γ (recall $\gamma = 2\epsilon\kappa$) provided that the ground-state dominance conditions are met. It is instructive to consider the asymptotic behaviors for weak and strong nematic interaction. For weak field strength ($\gamma \ll 1$), the correlation lengths in the two directions are $\xi_\perp = \xi_\parallel = \epsilon$, as expected, since $\mathcal{E}_0^0 = 0$ and $\mathcal{E}_1^1 = \mathcal{E}_1^0 = 2$ at $\gamma = 0$. In the limit of strong nematic interaction ($\gamma \gg 1$), we make use of the asymptotic behavior of $\mathcal{E}_l^m$ (Refs. 20 and 40) and find

$$\xi_\perp = \frac{\epsilon}{\gamma^{1/2}\left(1 - \frac{1}{2\gamma^{1/2}} - \mathcal{O}(\gamma^{-1})\right)}, \tag{43}$$

$$\xi_\parallel = \frac{\epsilon \exp(2\gamma^{1/2})}{16\gamma\left(1 - \frac{1}{\gamma^{1/2}} - \mathcal{O}(\gamma^{-1})\right)}. \tag{44}$$

The leading order term in these asymptotic expressions recover the scaling behavior of these two correlation lengths given in previous studies.[30–33] Note that the chain deformation in the nematic phase is characterized by an exponential growth of $\xi_\parallel$ in the field strength γ and an algebraic decay of $\xi_\perp$. The large discrepancy in the chain geometry has been demonstrated experimentally,[13] clearly showing the elongation of the chain in the direction of nematic ordering.

In Fig. 6, we show the behavior of $\xi_\perp$ (solid line) and $\xi_\parallel$ (dashed line) versus the field strength γ using the exact solutions given by Eqs. (41) and (42). In the isotropic phase ($\gamma = 0$), the two correlation lengths are equal, and, as we increase the nematic interaction from zero, the two correlation lengths split. For $\gamma > 10$, we see the correlation lengths rapidly diverge from each other, indicative of the coil-to-stretch transition. The asymptotic behavior given by the leading-order term in Eq. (43) (dot-dashed line) and Eq. (44) (dotted line), respectively, are included in Fig. 6 for large γ, which converge on our exact solutions near $\gamma = 100$. Figure 6 illustrates the usefulness of our results in capturing the chain statistical behavior in the intermediate-field-strength regime, which is important in describing the chain behavior under experimentally relevant conditions.

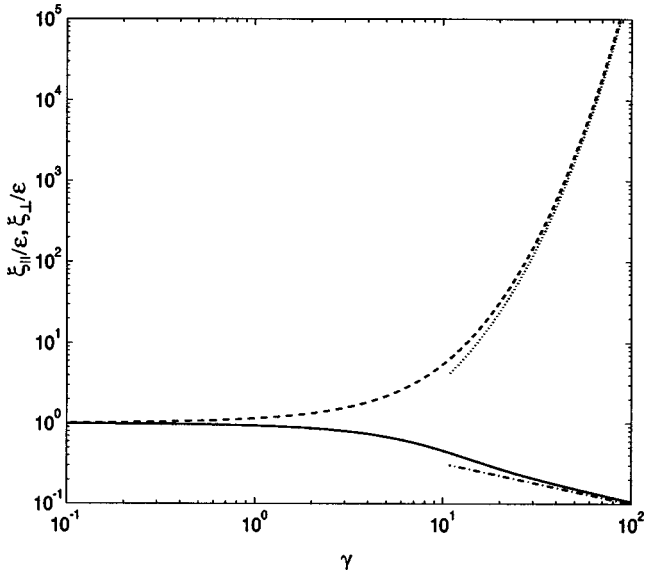

FIG. 6. The perpendicular correlation length $\xi_\perp/\epsilon$ (solid line) and parallel correlation length $\xi_\parallel/\epsilon$ (dashed line) vs the field strength γ from Eqs. (41) and (42), respectively. The asymptotic behavior of $\xi_\perp$ (dot-dashed line) and $\xi_\parallel$ (dotted line), given by the leading-order term in Eqs. (43) and (44), respectively, are included for large γ.

Following Ref. 33, we construct a general expression for $\langle u_i(\tau_1) u_j(\tau_2) \rangle$ making use of the correlation lengths $\xi_\perp$ and $\xi_\parallel$ that are consistent with the definition of the order parameter m[33]

$$\langle u_i(\tau_1) u_j(\tau_2) \rangle = \frac{\delta_{ij} - \delta_{i3}\delta_{j3}}{3}(1-m)\exp\left(-\frac{|\tau_1 - \tau_2|}{\xi_\perp}\right) + \frac{\delta_{i3}\delta_{j3}}{3}(1+2m)\exp\left(-\frac{|\tau_1 - \tau_2|}{\xi_\parallel}\right). \tag{45}$$

We comment that while this expression recovers the exact known result in the isotropic state, it is only valid for sufficiently long chain or large field strength in the nematic state. The reason is that in the nematic state the end portions of the chain behave differently from the mid portion; the difference becomes insignificant only in the long chain or large field strength limit. Mathematically this limit is equivalent to the ground-state dominance condition discussed in Sec. III. Combining the ground-state dominance criterion [Eq. (31)] with the general expression for the correlation length in the perpendicular direction Eq. (43), we find that the condition becomes simply $L \gg \xi_\perp$.[53] Using Eq. (45) in Eq. (39) and noting the condition $L \gg \xi_\perp$, we obtain

$$\langle R_i R_j \rangle = \frac{2}{3}(\delta_{ij} - \delta_{i3}\delta_{j3})(1-m)\xi_\perp L + \frac{1}{3}\delta_{i3}\delta_{j3}(1+2m) \times \left\{ 2\xi_\parallel L - 2\xi_\parallel^2 \left[1 - \exp\left(-\frac{L}{\xi_\parallel}\right) \right] \right\}. \tag{46}$$

The behavior of $\langle R_3^2 \rangle$ (parallel direction) shows a scaling cross-over from L^2 to L at $L \sim \xi_\parallel$ caused by the emergence of hairpin defects in the chain conformation; thus the correla-

Downloaded 14 Dec 2005 to 131.215.225.9. Redistribution subject to AIP license or copyright, see http://jcp.aip.org/jcp/copyright.jsp

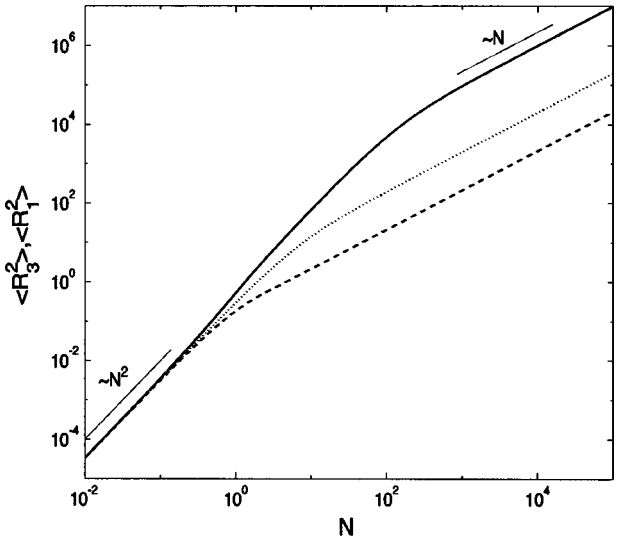

FIG. 7. The mean square end-to-end distance in the nematic and the perpendicular directions vs the chain length for fixed $\epsilon=\kappa=3$. The figure shows $\langle R_3^2\rangle$ (solid line) and $\langle R_1^2\rangle$ (dashed line) plotted with the isotropic solution (dotted line) given by Eq. (40), with appropriate scalings included.

tion length $\xi_\parallel$ can be identified as the average length between hairpin defects for a polymer chain in a uniform nematic phase.

In Fig. 7, we show the behavior of the mean square end-to-end distance [Eq. (39)] for a range of chain lengths at a fixed value of $\epsilon=\kappa=3$, which is consistent with the order of magnitude of the parameters in Figs. 2–4. The plot shows $\langle R_3^2\rangle$ (solid line) and $\langle R_1^2\rangle$ (dashed line) together with the isotropic solution (dotted line) [Eq. (40)] as a function of the nondimensionalized chain length N (recall $N=LA/v$, where A is the cross-section area of the chain and v is the volume of a solvent molecule). Figure 7 shows three distinct regimes. For very short chains ($L<\xi_\perp$), the mean-square end-to-end distances in the transverse (1st) and longitudinal (3rd) directions are equal to the mean-square end-to-end distance in the isotropic phase and exhibit the ballistic N^2 scaling. For longer chains ($\xi_\perp<L<\xi_\parallel$), we see the separation between the end-to-end distances in the transverse and longitudinal directions due to the presence of nematic order. The chain conformation is essentially aligned in the nematic direction with small excursions in the transverse directions thus resulting in the ballistic scaling N^2 in the longitudinal direction and the diffusive scaling N in the transverse direction in this intermediate regime. In the final regime ($N>\xi_\parallel$), the end-to-end distance in the parallel direction now also scales as N due to the introduction of hairpin turns in the conformation that can be located anywhere along the chain with nearly equal probability.

Next we discuss the effect of the nematic interaction on the single-chain energetics. We define the free energy of a single chain $f_{\rm SC}=-\log[q/(4\pi)]$ relative to the isotropic phase in units of k_BT. There are two energy contributions to the free energy, the bending energy, $E_{\rm SC}^{\rm bend}$, and the energy due to alignment by the nematic field, $E_{\rm SC}^{\rm align}$, which can be obtained from

$$E_{\rm SC}^{\rm bend}=-\epsilon\left(\frac{\partial \log q}{\partial \epsilon}\right)_\kappa, \tag{47}$$

$$E_{\rm SC}^{\rm align}=-\kappa\left(\frac{\partial \log q}{\partial \kappa}\right)_\epsilon. \tag{48}$$

The single chain entropy $s_{\rm SC}$, in units of k_B, is calculated using the definition of the free energy $f_{\rm SC}=E_{\rm SC}^{\rm bend}+E_{\rm SC}^{\rm align}-s_{\rm SC}$. Since these thermodynamic quantities are relative to the isotropic phase, they all approach zero in the limit of $\kappa\to 0$.

Upon increasing κ from zero, all these thermodynamic quantities decrease: $E_{\rm SC}^{\rm align}$ obviously decreases as can be seen directly from the second term in the effective single-chain Hamiltonian Eq. (17). The increased degree of alignment suppresses the thermal wrinkles in the chain conformation, which reduces the bending energy $E_{\rm SC}^{\rm bend}$. The entropy $s_{\rm SC}$ is similarly reduced because of the reduction in the effective number of degrees of freedom associated with the thermal wrinkles. Finally, thermodynamic stability dictates the free energy $f_{\rm SC}$ must decrease as the alignment field strength increases.

In the limit of weak field strength κ, the partition function can be expanded in powers of κ. This is equivalent to a perturbation expansion around the isotropic state. Because of the rotational symmetry, the linear terms in the field κ vanish identically. Thus, the thermodynamic quantities all scale as κ^2 as the leading correction in the weak field limit.

In the limit of strong field strength κ, we can find the asymptotic behavior of the thermodynamic quantities using ground-state dominance of the partition function q [Eq. (33)], which is good for parameters satisfying Eq. (31). The limiting behavior of the free energy and the alignment energy is $f_{\rm SC}=E_{\rm SC}^{\rm align}=-2L\kappa/3+\mathcal{O}(\kappa^{1/2})$, and the bending energy and entropy approach $s_{\rm SC}=2E_{\rm SC}^{\rm bend}=-L\sqrt{2\kappa/\epsilon}+\mathcal{O}(\kappa^0)$ as $\kappa\to\infty$. Thus the free energy is dominated by the alignment energy and the relationship between the entropy and the bending energy is a manifestation of the equipartition theorem for the small transverse fluctuation of a nearly straight chain. In this strong field limit, it is more instructive to define changes in the thermodynamic quantities relative to the infinite field (perfectly aligned) state. Using the ground-state equations in Sec. III and the limiting behavior of $\xi_\perp$ [Eq. (43)], we find

$$\frac{\Delta f_{\rm SC}}{f_{\rm SC}}\sim\frac{\Delta E_{\rm SC}^{\rm align}}{E_{\rm SC}^{\rm align}}\sim\frac{\Delta E_{\rm SC}^{\rm bend}}{E_{\rm SC}^{\rm bend}}\sim\frac{\Delta s_{\rm SC}}{s_{\rm SC}}\sim\frac{\xi_\perp}{\epsilon}, \tag{49}$$

where $\Delta f_{\rm SC}=f_{\rm SC}-f_{\rm SC}(\kappa\to\infty)$ (similarly for the other quantities). Thus in the strong field limit, the relative change in the thermodynamic quantities with reference to the perfectly aligned state scales as the ratio of the transverse correlation length to the natural persistence length of the chain. This scaling reflects the importance of the small amplitude fluctuations in the transverse directions for the single-chain thermodynamics in this limit. Since the longitudinal correlation length $\xi_\parallel$ does not appear at the leading order, hairpin defects do not play a significant role in the thermodynamic quantities, even though they play a key role in determining the chain size. The reason is that in the strong field limit, $\xi_\parallel$ is

Downloaded 14 Dec 2005 to 131.215.225.9. Redistribution subject to AIP license or copyright, see http://jcp.aip.org/jcp/copyright.jsp

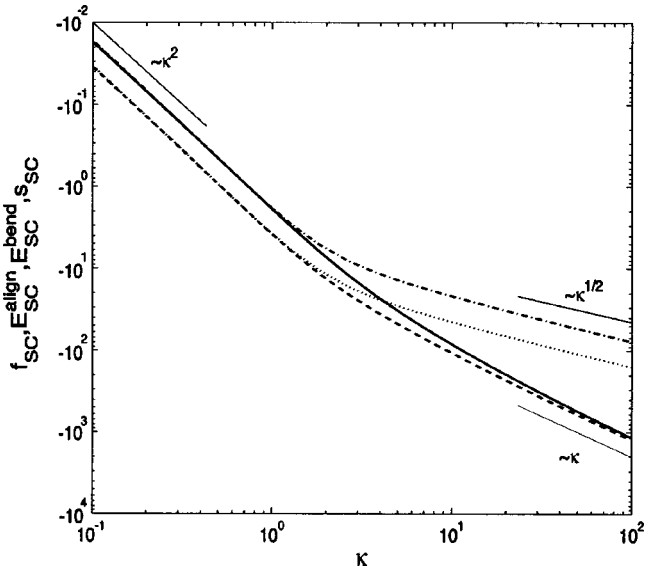

FIG. 8. The behavior of the free energy f_{SC} (solid line), the bending energy E_{SC}^{bend} (dot-dashed line), the alignment energy E_{SC}^{align} (dashed line), and the entropy (dotted line) of a single chain relative to the isotropic state as a function of the field strength κ for a fixed value of $N=20$ and $\epsilon=3$. Appropriate scalings in κ are included.

exponentially larger than $\xi_\perp$ [see Eqs. (43) and (44)], and hence the number of active degrees of freedom associated with the hairpin defects is exponentially small compared to the degrees of freedom due to the local transverse fluctuations.

In Fig. 8, we show the behavior of the single-chain free energy (solid line), the bending energy (dot-dashed line), the alignment energy (dashed line), and the entropy (dotted line) over a range of the field strength κ for a fixed chain length $N=20$ and persistence length $\epsilon=3$. The indicated scalings for large field strength κ are consistent with the limiting behaviors just described. The scaling cross-over evident in Fig. 8 is due to the freezing of the small amplitude conformation fluctuations that occurs as $\xi_\perp/\epsilon\to 0$. The crossover occurs at $\xi_\perp/\epsilon\sim 1$ or equivalently $\gamma\sim 1$.

VI. SUMMARY AND CONCLUSIONS

In this paper, we have studied the liquid crystalline polymer solution behavior by using a systematic self-consistent-field approach that simultaneously describes the solution thermodynamics and the single-chain statistical properties. The set of SCF equations are derived by using a field-theoretical approach and emerge as the lowest order approximation to the exact solution. The SCF theory reduces the many-chain problem to a single-chain in a self-consistent quadrupole field, which is then solved exactly using spheroidal functions.

As applications of the SCF theory, we have examined the phase behavior of the liquid-crystalline polymer solutions and calculated the single-chain conformation and thermodynamic properties in the nematic state. The interplay between the isotropic Flory–Huggins and anisotropic Maier–Saupe part of the two-body interaction leads to a variety of interesting phase diagrams. Analysis of the various spinodal curves in the phase diagram suggests rich and complex phase transition kinetics. For systems with sufficiently strong Flory–Huggins repulsive interactions between the polymer and the solvent, we point out several interesting situations where phase transition kinetics evolves along a multiple-step path that involves changes in the primary thermodynamic driving forces due to the coupling between concentration and nematic order. For example, for temperature quenches into certain part of the phase diagram we predict spinodal decomposition dynamics leading to isotropic–isotropic phase separation followed by subsequent nucleation of the nematic phase from the polymer-rich isotropic phase. When the polymer–solvent interaction is reduced, the critical point for isotropic–isotropic transition shifts inside the isotropic–nematic coexistence envelope thus becoming a metastable critical point. Just as in previous studies on colloidal systems and polymer crystallization with similar phase diagrams where it has been shown that the metastable critical point dramatically facilitates the formation of the crystalline phase near it, so here too we expect that the nucleation barrier for a liquid crystalline phase near a metastable critical point will be significantly reduced. By a comparison with the rigid-rod system, we find that chain flexibility significantly reduces the degree of nematic order even for quite stiff chains.

The single-chain statistics in the nematic state at the mean-field level is shown to be governed by only the natural persistence length of the polymer ϵ and a dimensionless nematic field strength $\gamma=2\epsilon a\phi_p mA$ where a is the strength of the Maier–Saupe interaction, ϕ_p the volume fraction of the polymer, m a normalized nematic order parameter, and A the cross-section area of the chain. Thus a given γ can correspond to multiple thermodynamic states of the polymer solution. The presence of a nematic field leads to the appearance of two length scales, a correlation length parallel to the nematic direction $\xi_\parallel$ and a correlation length perpendicular to the nematic direction $\xi_\perp$. Using ground-state dominance valid for sufficiently long chains, we provide exact results for these length scales that are valid for arbitrary field strengths and that reduce to the known results in the large field limit. In the strong field limit, these length scales correspond respectively to the average distance between hairpins and the persistence length for the fluctuation of the director in the transverse directions. Interestingly, we find that whereas hairpins play a critical role in determining the chain dimensions in the nematic state, it is the transverse fluctuations that dominate the single-chain thermodynamic properties in the strong field limit.

A major advantage of our approach is the systematicness with which mean-field theory is derived and the exact treatment of the chain statistics at the mean-field level. Our development of the self-consistent-field theory provides a natural framework for incorporating fluctuations, with the mean-field thermodynamic and single-chain properties calculated here serving as the essential input. In particular, the exact treatment of the chain statistics in the nematic state allows a nonperturbative treatment of the coupling between concentration and nematic order in the nematic phase. We have provided a cursory outline of the structure of the fluctuation theory for zero wave number or homogeneous concentration

Downloaded 14 Dec 2005 to 131.215.225.9. Redistribution subject to AIP license or copyright, see http://jcp.aip.org/jcp/copyright.jsp

and order parameter fluctuations and used this theory to determine the limit of metastability of the various phases. In a future publication, we will present the full fluctuation theory; such a theory will provide a nonperturbative, first-principles approach for computing the Frank elastic constants of a nematic polymer solution.

ACKNOWLEDGMENT

This work was supported in part by the National Science Foundation (DMR-9970589).

APPENDIX A: SPHEROIDAL FUNCTIONS

We have chosen to calculate the spheroidal functions by expanding them in terms of the more familiar spherical harmonics.[52] Application of recursive relations to the spherical harmonics results in

$$\cos\theta Y_l^m = A_l^{(+)m} Y_{l+1}^m + A_l^{(-)m} Y_{l-1}^m, \tag{A1}$$

where the coefficients are given by

$$A_l^{(+)m} = \left[\frac{(l-m+1)(l+m+1)}{(2l+1)(2l+3)}\right]^{1/2}, \tag{A2}$$

$$A_l^{(-)m} = \left[\frac{(l-m)(l+m)}{(2l-1)(2l+1)}\right]^{1/2}. \tag{A3}$$

The Hamiltonian matrix for our eigenvalue problem is given by

$$\begin{aligned}\langle Y_{l'}^{m'} | \mathcal{H} Y_l^m \rangle = {} & l(l+1)\delta_{l,l'}\delta_{m,m'} - \gamma[(A_l^{(+)m}A_{l+1}^{(-)m} \\ & + A_l^{(-)m}A_{l-1}^{(+)m})\delta_{l,l'} + A_l^{(+)m}A_{l+1}^{(+)m}\delta_{l+2,l'} \\ & + A_l^{(-)m}A_{l-1}^{(-)m}\delta_{l-2,l'}]\delta_{m,m'},\end{aligned} \tag{A4}$$

and the spheroidal functions are found by inversion of the Hamiltonian matrix, which is written in expansion form as

$$Ysp_l^m = \sum_{n=0}^{\infty} a_{l,n}^{|m|} Y_n^m. \tag{A5}$$

We note within the expansion that evaluation of $\cos^2\theta Y_l^m$ results in spherical harmonics with the l index raised and lowered by 2 and the m index unaffected, thus the expansion of the spheroidal functions into spherical harmonics does not require a summation over an m index. Furthermore, the summation over n in the expansion only requires the same parity functions to show up, meaning that for odd l, the summation need only include odd n, and for even l, the summation need only include even n.

The spherical harmonics are an orthonormal basis set of the form

$$\int d\boldsymbol{u} Y_l^m Y_{l'}^{m'*} = \delta_{l,l'}\delta_{m,m'}, \tag{A6}$$

furthermore, the complex conjugate of a spherical harmonic satisfies

$$Y_l^{m*} = (-1)^m Y_l^{-m}, \tag{A7}$$

thus the spheroidal functions and their coefficients satisfy

$$Ysp_l^{m*} = (-1)^m Ysp_l^{-m}, \tag{A8}$$

$$\sum_{n=0}^{\infty} a_{l,n}^{|m|} a_{l',n}^{|m|*} = \delta_{l,l'}. \tag{A9}$$

The numerical evaluation of the expansion coefficients requires truncation of the summation to a finite number of functions; however, as the ratio $L/(2\epsilon)$ grows large, only the first couple of eigenfunctions are necessary to accurately calculate the chain statistics. We have found agreement of the eigenvalues of the spheroidal functions given in current literature[41] when we sum the spherical harmonics up to an l-index of 150 for modest values of γ.

Numerical evaluation of the spheroidal functions allows for the evaluation of

$$q = 4\pi \sum_{l=0}^{\infty} C_l^0(L) |a_{l,0}^0|^2, \tag{A10}$$

$$m = \frac{3}{2L}\left(\frac{\partial \log q}{\partial \kappa}\right)_{\epsilon}, \tag{A11}$$

where $\kappa = a\phi_p mA$. In addition to the evaluation of the equilibrium potentials, knowledge of the chain statistics allows us to evaluate averages within the nematic phase.[20]

APPENDIX B: PERTURBATION PARTITION FUNCTION

An average quantity can be evaluated by integrating over all values of the quantity times the probability, which, depending on the complexity of the average, is quite difficult to perform numerically. For example, the average end-to-end distance in the z direction squared requires the evaluation of $\langle \cos\theta(\tau)\cos\theta(\tau')\rangle$, which contains three Green's functions in the integration: $G(\boldsymbol{u}_f|\boldsymbol{u}(\tau), L-\tau)$, $G(\boldsymbol{u}(\tau)|\boldsymbol{u}(\tau'), \tau-\tau')$, and $G(\boldsymbol{u}(\tau')|\boldsymbol{u}_0, \tau')$. After some simplifications, the quantity $\langle \cos\theta(\tau)\cos\theta(\tau')\rangle$ contains five summations in the numerical summation, which is extremely time consuming to calculate accurately. This is a very simple average in comparison to the averages that are necessary to account for density and order fluctuations in the free energy.[21]

Since we have already approximated the partition function by expanding the spheroidal functions in the spherical harmonics, we can calculate the partition function by adding a perturbation term to the Hamiltonian, thus rendering a partition function that acts as a generating function of the averages of interest. Specifically, we calculate the partition function for the Hamiltonian

$$\beta\mathcal{H}_\Delta = \beta\mathcal{H}_0 - \boldsymbol{\Delta}\cdot\int_0^L d\tau \boldsymbol{u}(\tau), \tag{B1}$$

which has chain statistics that satisfy

$$\begin{aligned}&\left[\frac{\partial}{\partial L} - \frac{1}{2\epsilon}\nabla_u^2 - a\phi_p mA\left(u_z u_z - \frac{1}{3}\right) - \boldsymbol{\Delta}\cdot\boldsymbol{u}\right] G(\boldsymbol{u}|\boldsymbol{u}_0, L) \\ &\quad = \delta(L)\delta(\boldsymbol{u}-\boldsymbol{u}_0).\end{aligned} \tag{B2}$$

Formulating the solution identically to the solution of the spheroidal functions, the eigenfunctions of this equation are

Downloaded 14 Dec 2005 to 131.215.225.9. Redistribution subject to AIP license or copyright, see http://jcp.aip.org/jcp/copyright.jsp

expanded in terms of the spherical harmonics. Application of recurrence relations to the spherical harmonics[52] results in

$$e^{i\phi}\sin\theta Y_l^m = -B_l^{(+)m} Y_{l+1}^{m+1} + B_l^{(-)m} Y_{l-1}^{m+1}, \tag{B3}$$

$$e^{-i\phi}\sin\theta Y_l^m = B_l^{(+)-m} Y_{l+1}^{m-1} - B_l^{(-)-m} Y_{l-1}^{m-1}, \tag{B4}$$

where the coefficients are given by

$$B_l^{(+)m} = \left[\frac{(l+m+1)(l+m+2)}{(2l+1)(2l+3)}\right]^{1/2}, \tag{B5}$$

$$B_l^{(-)m} = \left[\frac{(l-m)(l-m-1)}{(2l-1)(2l+1)}\right]^{1/2}. \tag{B6}$$

The resulting Hamiltonian matrix for our eigenvalue problem is

$$\begin{aligned}\langle Y_{l'}^{m'}|\mathcal{H}Y_l^m\rangle = {} & l(l+1)\delta_{l,l'}\delta_{m,m'} - \gamma[(A_l^{(+)m}A_{l+1}^{(-)m} + A_l^{(-)m}A_{l-1}^{(+)m})\delta_{l,l'} + A_l^{(+)m}A_{l+1}^{(+)m}\delta_{l+2,l'} + A_l^{(-)m}A_{l-1}^{(-)m}\delta_{l-2,l'}]\delta_{m,m'} \\ & + \frac{\Delta_x}{2}(B_l^{(+)m}\delta_{l+1,l'} - B_l^{(-)m}\delta_{l-1,l'})\delta_{m+1,m,'} - \frac{\Delta_x}{2}(B_l^{(+)-m}\delta_{l+1,l'} - B_l^{(-)-m}\delta_{l-l,l'})\delta_{m-1,m'} \\ & + \frac{\Delta_y}{2i}(B_l^{(+)m}\delta_{l+1,l'} - B_l^{(-)m}\delta_{l-1,l'})\delta_{m+1,m'} + \frac{\Delta_y}{2i}(B_l^{(+)-m}\delta_{l+1,l'} - B_l^{(-)-m}\delta_{l-1,l'})\delta_{m-1,m'} \\ & - \Delta_z(A_l^{(+)m}\delta_{l+1,l'} + A_l^{(-)m}\delta_{l-1,l'})\delta_{m,m'}. \end{aligned} \tag{B7}$$

Solving the eigenvalue problem, we expand the Green's function in terms of these new eigenfunctions, which can be integrated over the end orientations to yield the partition function q_Δ. Taking derivatives with respect to the perturbation field strength $\boldsymbol{\Delta}$ generates end-to-end averages, which we perform numerically.

[1] A. A. Collyer, *Liquid Crystal Polymers: From Structures to Applications* (Elsevier, New York, 1992).
[2] W. J. Zhou, J. A. Kornfield, V. M. Ugaz, W. R. Burghardt, D. R. Link, and N. A. Clark, Macromolecules **32**, 5581 (1999).
[3] N. Vaish, D. K. Cinader, W. R. Burghardt, W. Zhou, and J. A. Kornfield, Polymer **42**, 10147 (2001).
[4] V. M. Ugaz, W. R. Burghardt, W. J. Zhou, and J. A. Kornfield, J. Rheol. **45**, 1029 (2001).
[5] T. A. Ezquerra, E. López-Cabarcos, B. S. Hsiao, and F. J. Baltà-Calleja, Phys. Rev. E **54**, 989 (1996).
[6] K. Hongladarom, V. M. Ugaz, D. K. Cinader, W. R. Burghardt, J. P. Quintana, B. S. Hsiao, M. D. Dadmun, W. A. Hamilton, and P. D. Butler, Macromolecules **29**, 5346 (1996).
[7] A. Kagemoto, M. Nakazaki, S. Kimura, Y. Momohara, K. Ueno, and Y. Baba, Thermochim. Acta **284**, 309 (1996).
[8] Y. M. Evdokimov, T. V. Nasedkina, V. I. Salyanov, and N. S. Badaev, Mol. Biol. **30**, 219 (1996).
[9] S. G. Skuridin, A. T. Dembo, V. S. Efimov, and Y. M. Evdokimov, Dokl. Akad. Nauk **365**, 400 (1999).
[10] J. L. Sikorav, J. Pelta, and F. Livolant, Biophys. J. **67**, 1387 (1994).
[11] S. S. Zakharova, W. Jesse, C. Backendorf, and J. R. C. van der Maarel, Biophys. J. **83**, 1119 (2002).
[12] P. G. de Gennes, in *Polymer Liquid Crystals*, edited by A. Ciferri, W. R. Krigbaum, and R. B. Meyer (Academic, New York, 1982).
[13] M. H. Li, A. Brûlet, P. Davidson, P. Keller, and J. P. Cotton, Phys. Rev. Lett. **70**, 2297 (1993).
[14] M. Warner, J. M. F. Gunn, and A. B. Baumgartner, J. Phys. A **18**, 3007 (1985).
[15] J. V. Selinger and R. F. Bruinsma, J. Phys. II **2**, 1215 (1992).
[16] H. Fischer, A. Keller, and A. H. Windle, J. Non-Newtonian Fluid Mech. **67**, 241 (1996).
[17] O. Kratky and G. Porod, Recl. Trav. Chim. Pays-Bas **68**, 1106 (1949).
[18] W. Maier and A. Saupe, Z. Naturforsch. A **13**, 564 (1958).
[19] W. Maier and A. Saupe, Z. Naturforsch. A **14**, 882 (1959).
[20] X. J. Wang and M. Warner, J. Phys. A **19**, 2215 (1986).
[21] A. J. Liu and G. H. Fredrickson, Macromolecules **26**, 2817 (1993).
[22] S. Lee, A. G. Oertli, M. A. Gannon, A. J. Liu, D. S. Pearson, H. W. Schmidt, and G. H. Fredrickson, Macromolecules **27**, 3955 (1994).
[23] B. Y. Drovetsky, A. J. Liu, and C. H. Mak, J. Chem. Phys. **111**, 4334 (1999).
[24] A. M. Gupta and S. F. Edwards, J. Chem. Phys. **98**, 1588 (1993).
[25] G. A. Carri and M. Muthukumar, J. Chem. Phys. **109**, 11117 (1998).
[26] S. R. Zhao, C. P. Sun, and W. X. Zhang, J. Chem. Phys. **106**, 2520 (1997).
[27] W. X. Zhang, S. R. Zhao, and C. P. Sun, J. Chem. Phys. **106**, 2530 (1997).
[28] M. Pasquali, V. Shankar, and D. C. Morse, Phys. Rev. E **6402**, 020802 (2001).
[29] V. Shankar, M. Pasquali, and D. C. Morse, J. Rheol. **46**, 1111 (2002).
[30] T. Odijk, Macromolecules **19**, 2314 (1986).
[31] G. J. Vroege and T. Odijk, Macromolecules **21**, 2848 (1988).
[32] T. Odijk, J. Chem. Phys. **105**, 1270 (1996).
[33] A. Tkachenko and Y. Rabin, Macromolecules **28**, 8646 (1995).
[34] P. J. Flory, *Principles of Polymer Chemistry* (Cornell University Press, Ithaca, 1953).
[35] N. Schuld and B. A. Wolf, J. Polym. Sci., Part B: Polym. Phys. **39**, 651 (2001).
[36] R. P. Feynman and A. R. Hibbs, *Quantum Mechanics and Path Integrals* (McGraw-Hill, New York, 1965).
[37] G. H. Fredrickson, V. Ganesan, and F. Drolet, Macromolecules **35**, 16 (2002).
[38] M. W. Matsen, J. Phys.: Condens. Matter **14**, R21 (2002).
[39] H. Yamakawa, *Helical Wormlike Chains in Polymer Solutions* (Springer-Verlag, Berlin, 1997).
[40] J. Meixner and F. M. Schäfke, *Mathieusche Funktionen und Sphäroidfunktionen* (Springer, New York, 1954).
[41] L.-W. Li, M.-S. Leong, T. S. Yeo, P. S. Kooi, and K. Y. Tan, Phys. Rev. E **58**, 6792 (1998).
[42] L.-W. Li, X.-S. Kang, and M.-S. Leong, *Spheroidal Wave Functions in Electromagnetic Theory* (Wiley, New York, 2002).
[43] W. H. Press and B. P. Flannery, *Numerical Recipes* (Cambridge University Press, Cambridge, 1989).
[44] D. C. Morse and G. H. Fredrickson, Phys. Rev. Lett. **73**, 3235 (1994).
[45] P. G. de Gennes and J. Prost, *The Physics of Liquid Crystals* (Clarendon, Oxford, 1993).
[46] A. M. Lapeña, S. C. Glotzer, S. A. Langer, and A. J. Liu, Phys. Rev. E **60**, R29 (1999).

Downloaded 14 Dec 2005 to 131.215.225.9. Redistribution subject to AIP license or copyright, see http://jcp.aip.org/jcp/copyright.jsp

[47] J. T. Kindt and W. M. Gelbart, J. Chem. Phys. **114**, 1432 (2001).
[48] P. R. ten Wolde and D. Frenkel, Science **277**, 1975 (1997).
[49] V. Talanquer and D. W. Oxtoby, J. Chem. Phys. **109**, 223 (1998).
[50] P. D. Olmsted, W. C. K. Poon, T. C. B. McLeish, N. J. Terrill, and A. J. Ryan, Phys. Rev. Lett. **81**, 373 (1998).
[51] L. Onsager, Ann. N.Y. Acad. Sci. **51**, 627 (1949).
[52] G. B. Arfken and H. J. Weber, *Mathematical Methods for Physicists*, 4th ed. (Academic, New York, 1995).
[53] Inserting Eq. (43) into Eq. (31), we find an additional factor of $(\mathcal{E}_2^0 - \mathcal{E}_0^0)/(\mathcal{E}_1^1 - \mathcal{E}_0^0)$ in the criteria for ground-state dominance; however, this factor is of order 1 for all values of γ and does not alter the criteria.

Downloaded 14 Dec 2005 to 131.215.225.9. Redistribution subject to AIP license or copyright, see http://jcp.aip.org/jcp/copyright.jsp